Integration
geoscience
engineering
partnership
geoConvention 2013

SS-wave reflections from P-wave sources in azimuthally anisotropic media

James Gaiser*, formerly Geokinetics Inc., presently CGGVeritas, Houston, TX USA
and
Richard Verm, Geokinetics Inc., Houston, TX USA

Summary

Early theoretical and field studies showed that P-wave sources generate a substantial amount of shear-wave energy for pure-mode (SS-wave) exploration seismology. SV-waves are created in isotropic or VTI (vertical transversely isotropic) media by either buried explosives or surface vibrator and weight drop sources. These methods have not been embraced by our industry; however, benefits could include shallow S-wave velocity model building to help PS-wave processing (CMP processing is easier), and S-wave surface-consistent residual statics.

The purpose of this study is to re-examine the feasibility of recovering SS-waves generated by P-wave sources in azimuthally anisotropic media. We analyze 3D synthetic seismograms for VTI and HTI (horizontal transversely isotropic) media to demonstrate the analysis and retrieval of SS-waves. Using conventional PS-wave azimuth processing and analysis techniques, it is possible to recover both the fast and slow SV_1- and SV_2-waves related to vertically fractured media. Although fast and slow SH_1- and SH_2-waves are not excited by conventional P-wave sources in the anisotropy symmetry planes, these waves can also be recovered from paraxial azimuths up to $\pm$45 degrees. A field 3D-3C dataset over the Marcellus shale exhibits SS-waves and S-wave splitting for velocity/statics analyses.

Introduction

Early theoretical work (e.g., Miller and Pursey, 1954) showed that a vertical point force (P-wave source) on an isotropic free surface radiates SV-waves at high propagation angles from 30 to 60 degrees. Although SV-waves polarized in a vertical plane that includes the source are abundant, no SH-waves polarized in the horizontal plane are created. Also, there was much interest in the 1980s to harness S*-wave energy (Hron and Mikhailenko, 1981) from buried charges for exploration seismology in Europe and the United States. Fertig (1984) produced a rather good pure-mode (SS-wave) section from an explosive source at 18 m depth using these so-called S*-waves. These are SV-waves induced by the P-wave when it is excited near the free surface (Gutowski et al., 1984). Lash (1985) verified the generation of these waves in borehole experiments and indicated that a weight-drop or a vibrator source on the surface would also produce SV-waves.

Despite these early successes, the technique has not been embraced by our industry because there are a number of challenges. Most significantly, energy at vertical incidence is not generated to image reflectors directly below the source (Lash, 1985). In addition, two-way S-wave attenuation can result in low S/N data for deeper targets. Also, S-wave birefringence (splitting) in azimuthally anisotropic media is more difficult to process for 3D surveys.

The purpose of this study is to re-examine the feasibility of recovering SS-waves generated by P-wave sources in azimuthally anisotropic media. This is very important because anisotropy is a property of the earth, not the source that generates fast and slow S-waves. Given the drawbacks mentioned above, one benefit could be for shallow S-wave velocity model building. This is particularly useful for converted

P- to S-waves (PS-waves) where common-conversion point (CCP) processing is especially difficult at high angles of incidence. Common midpoint (CMP) processing is easier. Another useful application might be for S-wave surface-consistent residual statics. We generate synthetic seismograms for vertical transversely isotropic (VTI) and horizontal transversely isotropic (HTI) media to demonstrate the analysis and retrieval of SS-waves. A field 3D-3C dataset over the Marcellus shale exhibits SS-waves and S-wave splitting for velocity and statics analyses.

Modeling

Synthetic seismograms are computed using the program ANIVEC, a layer matrix, frequency-slowness integration algorithm (Mallick, 1987). Layers are laterally homogeneous but can be arbitrarily anisotropic. A 20x20, three-component (3C) receiver grid is centered over the shot location, which is a vertical point force, P-wave source. There is no random noise and attenuation is low.

Conventional PS-wave processing techniques are used to identify S-wave splitting. Fertig (1984) processed the inline horizontal component along a 2D line. For 3D we rotate to a source-centered coordinate system (Gaiser, 1999) of radial and transverse components and analyze azimuth stacks to find principal anisotropy directions. Rotation into these earth coordinates effectively separates data into fast and slow SS-waves for full offset and azimuth stacking.

Table 1: VTI Marcellus model. Depths and velocities are m and m/s, respectively, and density is gr/cm^3. The δ, ε and γ are Thomsen (1986) parameters.

Layer	*Depth*	V_{P0}	V_{S0}	ρ	δ	ε	γ
1 Genesee Shale	1323	4051	2203	2.67	0.05	0.075	0.05
2 Tully Limestone	1361	4962	2919	2.70	0.05	0.075	0.05
3 Hamilton Shale	1835	3866	2405	2.67	0.05	0.075	0.05
4 Marcellus Shale	1932	3235	2059	2.53	0.05	0.075	0.05
5 Onondaga Limestone	1977	4325	2501	2.64	0.05	0.075	0.05

VTI medium

The first model examined is a VTI simplification of the Marcellus shale play. It consists of five layers where the first reflection, at 1323 m deep, is from the top of the Tully limestone. Table 1 shows the model parameters for the five layers. Note that constant parameters are used for the anisotropy and there is little attenuation (Q=100). Figure 1 shows an example of a single receiver line along the inline direction (X) from the 3C shot-record. Colors highlight the P-wave (red), PS-wave (orange), and SS-wave (yellow) responses. The upper event is the combination of top and bottom Tully limestone, and the two lower events are the top and bottom of the Marcellus shale. Horizontal components show data from the inline (X) and crossline (Y) components, corresponding to particle motion U_X and U_Y from the acquisition coordinate system (Gaiser, 1999).

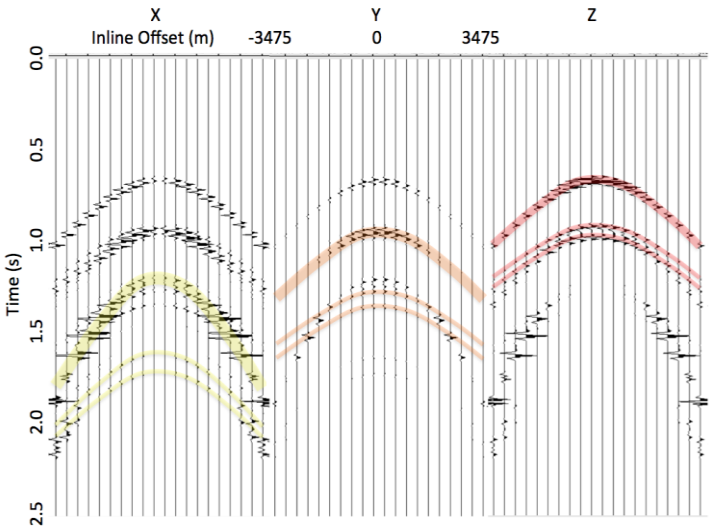

Figure 1: Three component synthetic seismograms from a VTI model of the Marcellus shale play. The source is a vertical point force to simulate a P-wave vibrator. Crossline offset is about 200 m. See text for explanation of highlighted events.

Processing consists of an SS-wave velocity analysis, constant velocity NMO corrections, and near offset stacking in 10 deg azimuth bins to assess the presence of S-wave splitting (Figure 2a). Although there are polarity rever-

sals in azimuth (dipole response) on both horizontal components, all reflections occur at constant traveltime, indicating no azimuthal anisotropy. Rotating to radial (U_R) and transverse ($U_\varnothing$) particle motion coordinates does not alter the amplitude of reflections, but shows the projection of their particle motion (Figure 2b), in a cylindrical coordinate system (Gaiser, 1999). Here it is clear that only SV-waves are present; all the particle motion is on U_R, in the vertical plane containing the source and receiver, and no response is on $U_\varnothing$. This is in agreement with S-wave radiation from Miller and Pursey (1954) in an isotropic or VTI medium. Only the SV-wave is generated by the source, as it is coupled with the P-wave. There are no transverse SS-waves.

The situation is very different in an azimuthally anisotropic medium shown next. Although the vertical source generates predominantly radial particle motion, SV- and SH-waves cannot propagate in general, except along the principal axes. However, in these directions there will only be a fast (SV_1-wave) and a slow (SV_2-wave). In azimuths between the principal axes, SV-waves and SH-waves don't exist, only a fast SS_1-wave and slow SS_2-wave with particle motion within the principal directions.

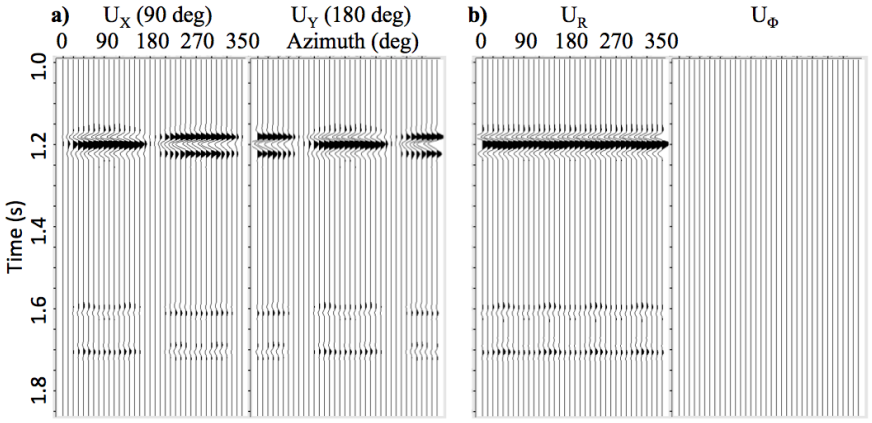

Figure 2: Common azimuth stack traces every 10 degrees of the SS-waves for the VTI synthetic data. Inline (U_X) and crossline (U_Y) particle motion (a), when receivers are oriented in the acquisition coordinates. Radial (U_R) and transverse ($U_\varnothing$) particle motion (b), when receivers are oriented in a source-centered (cylindrical) coordinate system. Clearly there are only SV-waves and no SH-waves.

HTI medium

Next, synthetic seismograms are computed for an HTI medium where the fast principal axis (symmetry plane) is oriented in the X direction at 90 deg and the slow direction (symmetry axis) is oriented in the Y direction at 180 deg. This corresponds to a single fracture set oriented east-west resulting in higher velocities in that direction.

Table 2 shows the model parameters for the same five layers. In this case there are two vertical S-wave velocities, SV_1-wave and SV_2-wave, with about 5% S-wave splitting anisotropy. The Thomsen (1986) parameters are the same as the VTI case but have the superscript (V), indicating they correspond to the azimuth of the vertical plane containing the symmetry axis. Velocities are isotropic in the azimuth containing the symmetry plane. These parameters correspond to a single set of fractures that are partially gas filled.

Processing follows the same method as for VTI data to create azimuth stacks of radial and transverse particle motion (Figure 3a). There are numerous events related to just 5% anisotropy. These are the constructive and destructive interference of SS_1- and

Table 2: HTI Marcellus model. Depths and velocities are in m and m/s, respectively, and density is gr/cm^3. There are two vertical S-wave velocities, fast V_{S1} and slow V_{S2}. The $\delta^{(V)}$, $\varepsilon^{(V)}$ and $\gamma^{(V)}$ are Thomsen (1986) parameters in the symmetry axis directions.

Layer	*Depth*	V_{P0}	V_{S1}	V_{S2}	ρ	$\delta^{(V)}$	$\varepsilon^{(V)}$	$\gamma^{(V)}$
1 Genesee Shale	1323	4051	2203	2093	2.67	0.05	0.075	0.05
2 Tully Limestone	1361	4962	2919	2773	2.70	0.05	0.075	0.05
3 Hamilton Shale	1835	3866	2405	2285	2.67	0.05	0.075	0.05
4 Marcellus Shale	1932	3235	2059	1956	2.53	0.05	0.075	0.05
5 Onondaga Ls	1977	4325	2501	2376	2.64	0.05	0.075	0.05

SS_2-waves detected on U_R and $U_\varnothing$, respectively. They are not propagating modes, except along the principal anisotropy directions. To obtain the fast and slow pure modes, first the principal directions are identified on $U_\varnothing$ at azimuths where polarity reversals occur (90 and 180 deg). Rotating into this earth coordinate system effectively separates these S-waves into SS_1- and SS_2-waves (Figure 3b). Here, U_{S1} and U_{S2} are the particle motions of the fast and slow pure-modes, where the time delay on U_{S2} is now clearly apparent, relative to U_{S1}. Note that there are still polarity reversals related to the dipole response of horizontal detectors.

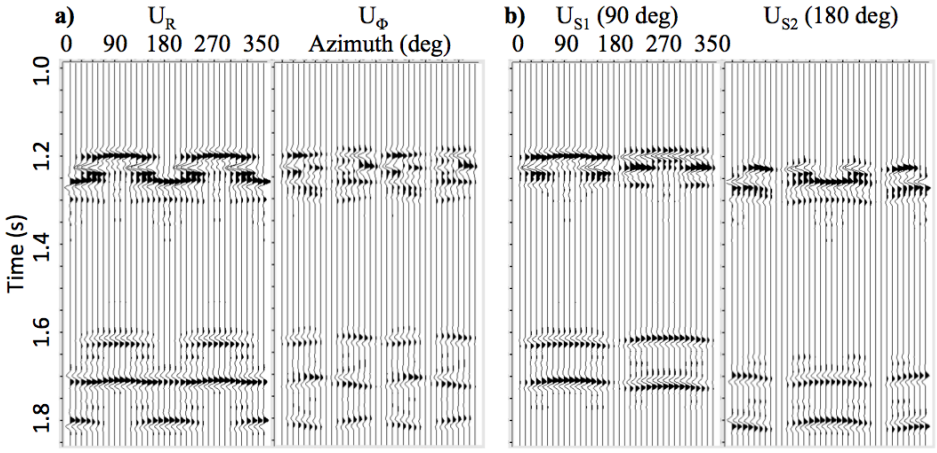

Figure 3: Common azimuth stack traces every 10 degrees of the SS-waves for the HTI synthetic data. Radial (U_R) and transverse ($U_\varnothing$) particle motion (a), when receivers are oriented in source-centered coordinates. Fast (U_{S1}) and slow (U_{S2}) particle motion (b), when receivers are oriented in the earth coordinate system to separate the pure-mode SS-waves.

Discussion

It is important to emphasize that radial and transverse particle motion coordinates for HTI media (Figure 3a) do not in general separate coherent SV- and SH-waves. In an azimuthally anisotropic medium, the response is a property of the earth's anisotropy coordinates between source and receiver. In isotropic or VTI media (Figure 2b), the radial does result in coherent SV-waves but there are no SH-waves on the transverse because the response is a property of the source. Recently, Hardage (2011) suggests that both SV- and SH-waves propagate away from a vertical point source in all directions in isotropic or VTI media. However, this does not agree with S-wave radiation theory and our results; there are no SH-waves, as seen on the transverse component of Figure 2b. Furthermore, if one erroneously assumes an isotropic or VTI media and performs an azimuth stack of radial and transverse data from an HTI medium (Figure 3), significant errors will result. The transverse component response tends to be minimal suggesting no SH-waves (polarity reversals neatly cancel everything), and the radial component response will result in a combination of fast and slow reflections.

This raises the interesting question of how to properly perform a full-azimuth stack of the separated data in azimuthally anisotropic media (Figure 3b). Again, a simple stack of the separated U_{S1} and U_{S2} data will result in cancelation because of the dipole response of horizontal detectors. In practice, shots on either side of a receiver tend to have opposite polarity for similar offsets. Figure 4 shows that a 180 deg rotation of half the data (180 to 360 deg for U_{S1}, and 270 to 90 deg for U_{S2}) corrects for the dipole response and polarity re-

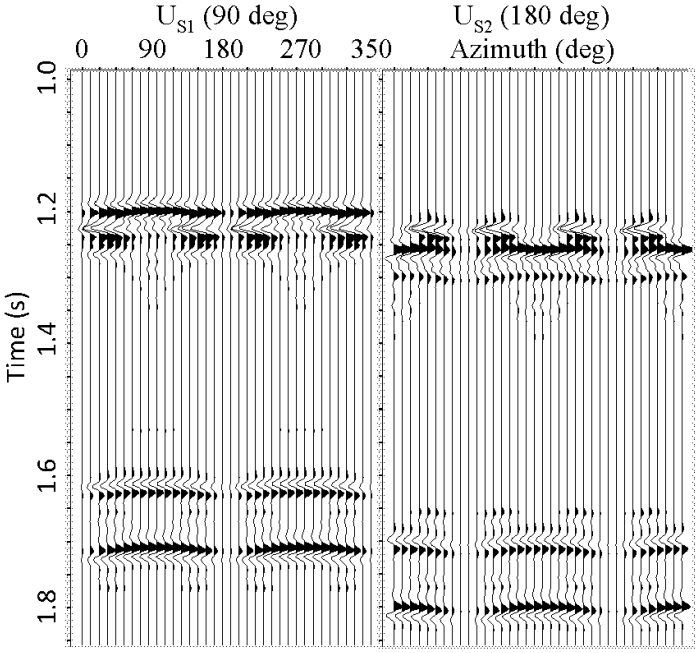

Figure 4: Fast (U_{S1}) and slow (U_{S2}) SS-wave azimuth stacks for the HTI synthetic data. Receivers are oriented in the earth coordinate system and the dipole response of horizontal detectors has been corrected.

versal (Gaiser, 1999). Stacking over azimuth after this additional rotation will result in an estimate of the fast and slow, SS_1- and SS_2-waves.

However, even this approach is an over simplification because it assumes that reflectivity of the fast or slow SS-waves is constant with azimuth. This is clearly not the case, as demonstrated by the null directions and amplitude variations with azimuth (AVAz) of the top and bottom Tully limestone reflection, the peak-trough at 1200 ms (Figure 4). For example, on the fast U_{S1} polarized SS_1-wave, after correction for polarity, the reflection character around 90 and 270 deg is very different compared with azimuths paraxial to 0 and 180 deg (±45 deg). This can result from differences in velocity (and reflection coefficient) between the fast and slow directions. Also, since the top and bottom of the Tully are very close to each other, tuning effects could be different for the fast and slow SS-waves. It is important to understand that the fast SS_1-wave varies from pure-mode SV_1-fast at 90 and 270 deg to pure-mode SH_1-fast at 0 and 180 deg. Note that SH_1-fast has zero amplitude precisely at 0 and 180 deg because a P-wave vertical point source does not produce SH-waves. A similar situation exists for the slow U_{S2} polarized SS_2-wave after correction for polarity (Figure 4). In this case the top Tully reflection (peak at 1250 ms) has a significant precursor that could be the result of fast and slow SS-wave interference in azimuths between the principal directions. Its character is similar to the bottom Tully reflection on the fast U_{S1} component. Nevertheless, we would ideally like to retrieve all four wavefields from P-wave source data: SV_1-fast, SV_2-slow, SH_1-fast and SH_2-slow (likewise for converted wave modes: PSV_1-fast, PSV_2-slow, PSH_1-fast and PSH_2-slow). Limited azimuth stacks of ±45 deg about the principal axes could achieve an estimate of the four SS-waves.

Marcellus field data

The techniques described here should also hold for data collected in media with orthorhombic anisotropy (a combination of VTI and HTI) and is more realistic of a layered medium with a single set of fractures. Two sets of fractures can also result in orthorhombic symmetry as the Marcellus shale exhibits in Pennsylvania. Here, the fractures are oriented at 90 deg with each other. The Marcellus field 3D-3C data exhibits good PS-waves where S-wave splitting analyses indicate a N80E fast direction (Gaiser et al., 2011).

Horizontal components of the Marcellus data were processed for the fast and slow SS-waves (Figure 5). Constant velocity analyses, surface-consistent deconvolution, NMO corrections, and surface-consistent statics were performed. A rotation of the horizontal components about the vertical axis separated data into fast (N80E) and slow (N170E) SS-waves before stacking. Although the S/N of SS-waves is lower than the PS-waves, the fast SS-wave data has a better S/N than the slow SS-wave data, similar to the PS-wave data. Several issues were not addressed here in the processing of the synthetic or field data. In practice, attenuation of SS-waves can be high, and S/N is often low because of interfer-

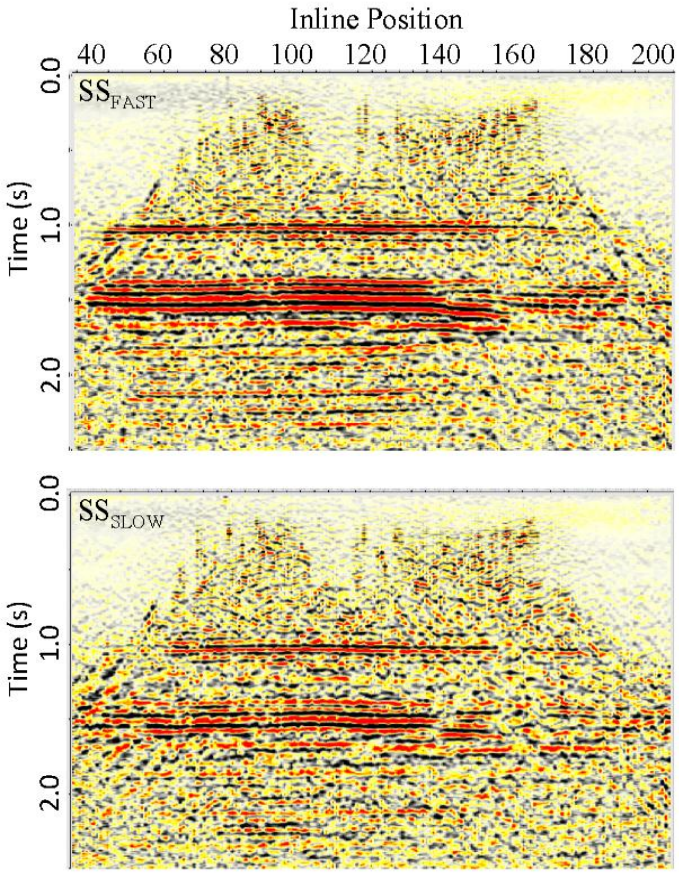

Figure 5: Fast and slow SS-wave stacks after surface consistent deconvolution and residual statics. These are stacks of all azimuths after the components were rotated to N80E and N170E.

ence with coherent surface waves. Also, no random noise was added to the synthetic data, and AVO effects of SV-wave reflections at near angles of incidence are not accounted for in the stacks. Finally, variations in azimuthal NMO (observed in the synthetic data in Figure 4) were not taken into account and could be a factor to include in the processing.

Conclusions

Synthetic seismograms of SS-waves from P-wave sources, computed for azimuthally anisotropic media, can be processed similar to PS-waves for the fast and slow SS-modes. The 3D-3C dataset over the Marcellus shale exhibits SS-waves and S-wave splitting for velocity and statics analyses, similar to PS-waves.

Acknowledgements

We thank Suat Altan for his expertise and help with the Marcellus data processing. Also, thanks go to Geokinetics and Geophysical Pursuit (co-owners of the Marcellus data) for permission to publish. This study was first presented in 2012 at the EAGE and SEG annual conferences. We are grateful to the CSEG for the opportunity to present it at the GeoConvention 2013 as a Best of SEG contribution.

References

Fertig, J., 1984, Shear waves by an explosive point-source: the earth surface as a generator of converted P-S waves: Geophysical Prospecting, **32**, 1–17.

Gaiser, J.E., 1999, Applications for vector coordinate systems of 3-D converted-wave data: The Leading Edge, **18**, 1290–1300.

Gaiser, J., A. Chaveste, M. Edrich, T. Rebec and R. Verm, 2011, Seismic anisotropy of the Marcellus shale: feasibility study for fracture characterization: CSEG CSPR CWLS Convention, Expanded Abstract.

Gutowski, P.R., F. Hron, D.E. Wagner, and S. Treitel, 1984, S*: Bulletin of the Seismological Society of America, **74**, 61–78.

Hardage, R., 2011, System and method for acquisition and processing of elastic wavefield seismic data: United States patent, **8,040,754 B1**, 1–30.

Hron, F. and B. Mikhailenko, 1981, Numerical modeling of nongeometrical effects by the Alekseev-Mikhailenko method: Bulletin of the Seismological Society of America, **71**, 1011–1029.

Lash, C., 1985, Shear waves produced by explosive sources: Geophysics, **50**, 1399–1409.

Mallick, S. and L.N. Frazer, 1987, Practical aspects of reflectivity modelling: Geophysics, **52**, 1355–1364.

Miller, G.F. and H. Pursey, 1954, The field and radiation impedance of mechanical radiators on the free surface of a semi-infinite isotropic solid: Proceedings of the Royal Society, **A223**, 521–541.

Thomsen, L., 1986, Weak elastic anisotropy: Geophysics, **51**, 1954–1966.